A Complex-Frequency Framework for Kerker Unidirectionality in Photonic Resonators (Supplementary Information)

Loubnan Abou-Hamdan,[1] Aloke Jana,[1] Rémi Colom,[2] Nour Abouyoussef,[1,3] Cooper Carlson,[1] Adam Overvig,[4] Felix Binkowski,[5] Sven Burger,[5,6] and Patrice Genevet[a)1]

[1)] *Department of Physics, Colorado School of Mines, 1523 Illinois Street, Golden, CO 80401, USA*

[2)] *Université Côte d'Azur, CNRS, CRHEA, 06560 Valbonne, France*

[3)] *Sibley School of Mechanical and Aerospace Engineering, Cornell University, 124 Hoy Road, Ithaca, NY 14850, USA*

[4)] *Stevens Institute of Technology, 1 Castle Point Terrace, Hoboken, NJ 07030, USA*

[5)] *Zuse Institute Berlin, 14195 Berlin, Germany*

[6)] *JCMwave GmbH, 14050 Berlin, Germany*

[a)] Corresponding author: patrice.genevet@mines.edu

Contents

I Finite-element method electromagnetic simulations and contour integration

Supporting Figure 1a shows the 64 discretized contour integration points (red circles), which have been used to numerically compute the contour integrals. This particular example is shown for a height $h = 150$ nm of the silicon cylinders, which corresponds to the full backward scattering condition (Kerker 2). The black crosses represent two fundamental resonance modes, or poles, corresponding to the resonator's magnetic and electric dipoles at $\omega = (1.973 - 0.041i) \times 10^{15}$ s^{-1} and $\omega = (1.855 - 0.023i) \times 10^{15}$ s^{-1}, respectively. In this specific parameter choice, we observe that zeros of the reflection coefficient are complex conjugates of each other, as described in the main text. This method of calculating poles and zeros using the contour integral approach was utilized to study the evolution of the position of the scattering coefficient singularities in the complex frequency plane as a function of the nanoresonator height. Supporting Fig. 1b illustrates the evolution of reflection and transmission poles and zeros (T- and R-zeros) as a function of height $h \in [75\,\text{nm}, 300\,\text{nm}]$.

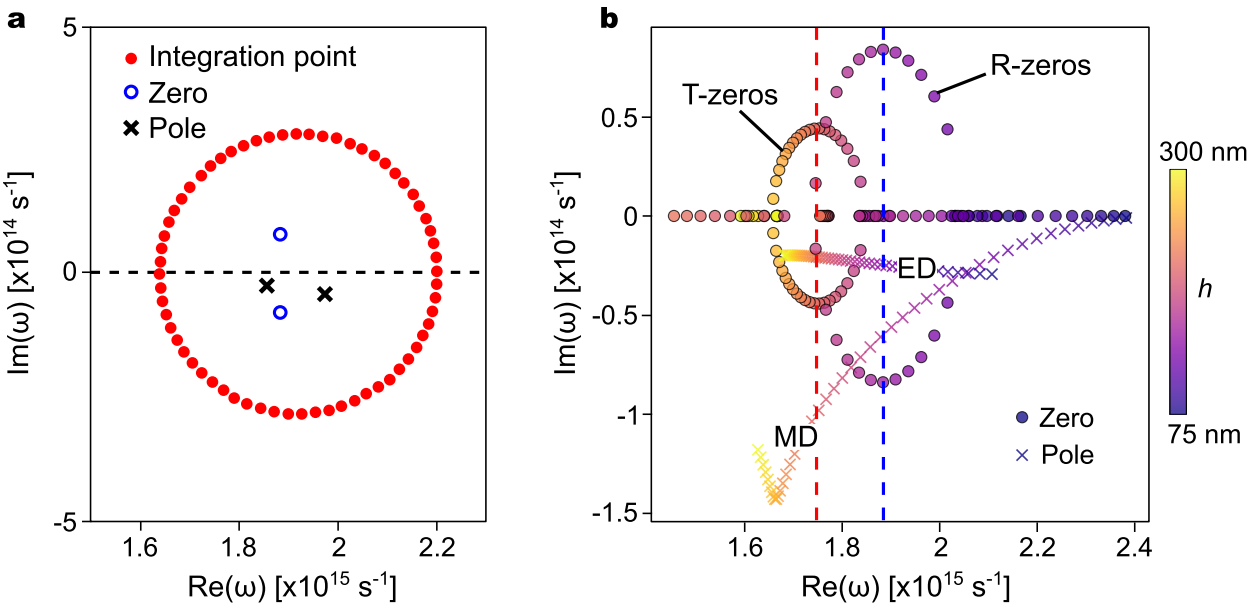

Supporting Fig. 1. **a**, Calculation of the poles and zeros of the scattering coefficients using the contour integration method. **b**, The evolution of the poles and zeros in the complex-frequency plane with variable height $h \in [75\,\text{nm}, 300\,\text{nm}]$ of the silicon meta-atoms.

A Real versus complex frequency crossing at the Huygens condition

The parametric evolution of the fundamental resonances, namely the electric dipole (ED) and magnetic dipole (MD) modes, is observed in the complex-frequency plane (see Supporting Fig. 1b, crosses). Initially, the MD resonance appears at a higher excitation frequency compared to the ED mode, starting from $h = 75$ nm. However, as the nanoresonator height increases, the MD mode spectrally shifts at a faster rate than the ED, keeping all other geometric parameters, such as period and diameter, fixed. At a critical height of $h = 195$ nm, the resonances cross each other at a real frequency of 1.77×10^{15} Hz, as indicated by the red dashed line in Supporting Fig. 1b. This crossing satisfies the classical condition of Huygens' sources, where two resonant modes with equal amplitudes but opposite symmetry were described to spectrally overlap, resulting in a fully transmissive device[1].

It is important to emphasize that in a realistic experiment, the spectral overlap does not occur, particularly in the complex plane. We observe that only the real frequency values of the complex poles cross. We thus studied the problem in greater depth and demonstrated that having identical real frequency is an insufficient condition for realizing Huygens' sources.

For instance, the presence of a T-zero near the real frequency axis, particularly one close to the operating frequency, can lead to significant loss of transmission, thereby preventing the resonator from functioning as a Huygens' source. Therefore, a thorough investigation of the evolution of zeros in the complex plane is essential for a complete understanding of the unidirectional scattering behavior. The necessary conditions for full backward scattering require that the system operates within the $\mathcal{PT}$-broken regime of the R-zeros and that a nearby pole is present. In both Kerker 1 and Kerker 2 scenarios, a resonance mode (in this case, the ED mode) with a high-quality factor exists within the $\mathcal{PT}$-broken regime, serving as the source term for unidirectional scattering.

II Transmission and reflection zeros as eigenvalue-degeneracies of the scattering and transfer matrices

In this section, we show that the zeros of the transmission and reflection coefficients correspond to the spectral positions at which the eigenvalues of the scattering and transfer matrices of a photonic system are degenerate.

The scattering matrix of a photonic system with mirror symmetry is expressed as

$$S = \begin{pmatrix} S_{11} & S_{12} \\ S_{21} & S_{22} \end{pmatrix} = \begin{pmatrix} r & t \\ t & r \end{pmatrix}, \tag{1}$$

in which r and t are the reflection and transmission coefficients of the system. The eigenvalues of the scattering matrix given above are

$$\Lambda_S^{\pm} = r \pm t. \tag{2}$$

Thus, the eigenvalues of the scattering matrix are degenerate and unimodular when $t = 0$ (since $|r| \to 1$ when $t \to 0$), *i.e.*, at the zeros of the transmission coefficient. The normalized eigenvectors corresponding to these eigenvalues are

$$\Phi_S^{\pm} = \frac{1}{\sqrt{2}} \begin{pmatrix} 1 \\ \pm 1 \end{pmatrix}. \tag{3}$$

The scattering matrix relates outgoing waves to incoming waves in the photonic system under consideration, $s_- = S s_+$ (where s_+ and s_- are the incoming and outgoing waves,

respectively). To relate the fields on the left-hand side of the photonic system to those on the right-hand side, on the other hand, we must evaluate the system's transfer matrix. The transfer matrix M is obtained from the entries of the scattering matrix as follows[2]

$$M = \begin{pmatrix} S_{21} - \frac{S_{22}S_{11}}{S_{12}} & \frac{S_{22}}{S_{12}} \\ -\frac{S_{11}}{S_{12}} & \frac{1}{S_{12}} \end{pmatrix} = \begin{pmatrix} t - \frac{r^2}{t} & \frac{r}{t} \\ -\frac{r}{t} & \frac{1}{t} \end{pmatrix}. \tag{4}$$

The eigenvalues of this transfer matrix are

$$\Lambda_M = \frac{t^2 - r^2 + 1}{2t} \pm \frac{1}{2t}\sqrt{\left[t^2 - r^2 + 1\right]^2 - 4t^2}. \tag{5}$$

These eigenvalues are degenerate and unimodular if $r = 0$ and $t = 1$. The eigenvetors of the transfer matrix are

$$\Phi_M^{\pm} = \left(-\frac{-1 - r^2 + t^2 \pm \sqrt{1 - 2r^2 + r^4 - 2t^2 - 2r^2t^2 + t^4}}{2r} \quad 1 \right)^{\mathrm{T}}. \tag{6}$$

When $r \to 0$ we have $|t| \to 1$, but t may still carry a phase. Assuming for simplicity that $t \to 1$ in the vicinity of $r = 0$, then the eigenvectors of the transfer matrix become

$$\Phi_M^{\pm} = \mp i \Phi_{\pm}, \tag{7}$$

where $\Phi_{\pm} = (1 \quad \pm i)^{\mathrm{T}}$ are the right- and left-circularly polarized eigenstates.

III Temporal coupled-mode theory (TCMT) of multi-mode photonic resonators

A TCMT of a two-mode, two-port resonator

We consider a photonic system that exhibits multiple resonant modes whose resonance frequencies and decay rates are represented by the $n \times n$ matrices Ω_0 and Γ, respectively, where n is the number of modes. The dynamic equations describing the photonic system's resonance amplitudes Ψ $(n \times 1)$ are expressed as[3,4]

$$\frac{\mathrm{d}\Psi}{\mathrm{d}t} = (-i\Omega_0 - \Gamma)\Psi + \kappa^{\mathrm{T}} s_+, \tag{8}$$

$$s_- = S_{\mathrm{d}} s_+ + C_\Psi \Psi. \tag{9}$$

In the above equations, s_+ and s_- are $m \times 1$ matrices (m is the number of ports) giving the incoming and outgoing waves, respectively, S_d is an $m \times m$ unitary matrix associated with the direct transport process of light (*e.g.*, specular reflection), C_Ψ is an $m \times n$ matrix corresponding to resonant scattering from the system, and κ is an $m \times n$ matrix giving the coupling coefficients of the modes. For a $\mathcal{PT}$-symmetric photonic system, these matrices satisfy the following relations[5]

$$C_\Psi^\dagger C_\Psi = 2\Gamma, \tag{10}$$

$$\kappa = C_\Psi, \tag{11}$$

$$S_\mathrm{d} C_\Psi^* = -C_\Psi. \tag{12}$$

Note that the mode amplitude is normalized so that $|\Psi|^2$ gives the resonator energy. In addition, it is assumed that the modes evolve harmonically in time, following the time dependence $e^{-i\Omega t}$ so that the mode frequencies are given by $\Omega_0 - i\Gamma$. Using this time dependence in Eq. (8), we obtain the following resonance amplitude

$$\Psi = (-i\Omega + i\Omega_0 + \Gamma)^{-1} \kappa^\mathrm{T} s_+, \tag{13}$$

where Ω is an $n \times n$ diagonal matrix whose entries are the excitation frequencies. Utilizing this solution in Eq. (9) yields the following scattering matrix

$$S = S_\mathrm{d} + C_\Psi (-i\Omega + i\Omega_0 + \Gamma)^{-1} \kappa^\mathrm{T}. \tag{14}$$

Using Eqs. (11) and (12) and the fact that S_d is unitary we can rewrite the scattering matrix as follows

$$S = \left\{ I - i\kappa \Big[\Omega - (\Omega_0 - i\Gamma) \Big]^{-1} \kappa^\dagger \right\} S_\mathrm{d}, \tag{15}$$

where I is the $m \times m$ identity matrix. The term between parentheses above can be rewritten using Eqs. (10) and (11) as $H_0 = \Omega_0 - i\kappa^\dagger \kappa / 2$.

The considered two-port metasurface supports two modes of opposite symmetry, an electric dipolar mode and a magnetic dipolar mode, and is thus equivalent to a photonic system with $n = m = 2$, which is described by the following matrices

$$\Omega_0 = \begin{pmatrix} \omega_1 & 0 \\ 0 & \omega_2 \end{pmatrix}, \quad \Gamma = \begin{pmatrix} \gamma_1 & \gamma_0 \\ \gamma_0^* & \gamma_2 \end{pmatrix}, \quad S_{\mathrm{d}} = \begin{pmatrix} r_0 & it_0\sqrt{\frac{n_{\mathrm{eff}}}{n_{\mathrm{air}}}} \\ it_0\sqrt{\frac{n_{\mathrm{eff}}}{n_{\mathrm{air}}}} & r_0 \end{pmatrix},$$
$$\text{and} \quad C_\Psi = \begin{pmatrix} C_{11\Psi} & C_{12\Psi} \\ C_{21\Psi} & C_{22\Psi} \end{pmatrix}. \tag{16}$$

The Fresnel reflection and transmission coefficients r_0 and t_0 corresponding to the direct transport process for p-polarized light that is normally incident upon the metasurface are given by

$$r_0 = \frac{n_{\mathrm{eff}} - n_{\mathrm{air}}}{n_{\mathrm{eff}} + n_{\mathrm{air}}} \quad \text{and} \quad t_0 = \frac{2n_{\mathrm{air}}}{n_{\mathrm{eff}} + n_{\mathrm{air}}}, \tag{17}$$

where $n_{\mathrm{eff}} = \sqrt{\varepsilon_{\mathrm{eff}}}$ is the effective index of refraction of the metasurface and $n_{\mathrm{air}} = 1$. In what follows, we will use the definition $t_0' = it_0\sqrt{\frac{n_{\mathrm{eff}}}{n_{\mathrm{air}}}}$ to lighten the notations.

Applying Eq. (10), we get

$$|C_{11\Psi}| = |C_{21\Psi}| = \sqrt{\gamma_1}, \tag{18}$$
$$|C_{12\Psi}| = |C_{22\Psi}| = \sqrt{\gamma_2}. \tag{19}$$

Since the structure has mirror symmetry and the two modes have opposite symmetry, then $\gamma_0 = 0$ (see Ref.[5]) and from Eqs. (18) and (19) we have the following relations between the entries of C_Ψ

$$C_{11\Psi} = \pm C_{21\Psi}, \tag{20}$$
$$C_{12\Psi} = \mp C_{22\Psi}, \tag{21}$$

where the top (bottom) signs are used when the first (second) mode is even and the second (first) mode is odd. Using the above relations in Eq. (12) yields

$$C_\Psi = \kappa = \begin{pmatrix} \pm i\sqrt{\gamma_1(r_0 \pm t_0')} & \mp i\sqrt{\gamma_2(r_0 \mp t_0')} \\ i\sqrt{\gamma_1(r_0 \pm t_0')} & i\sqrt{\gamma_2(r_0 \mp t_0')} \end{pmatrix}. \tag{22}$$

It can be readily verified that the above expression for C_Ψ satisfies Eq. (10) with $\gamma_0 = 0$ as required.

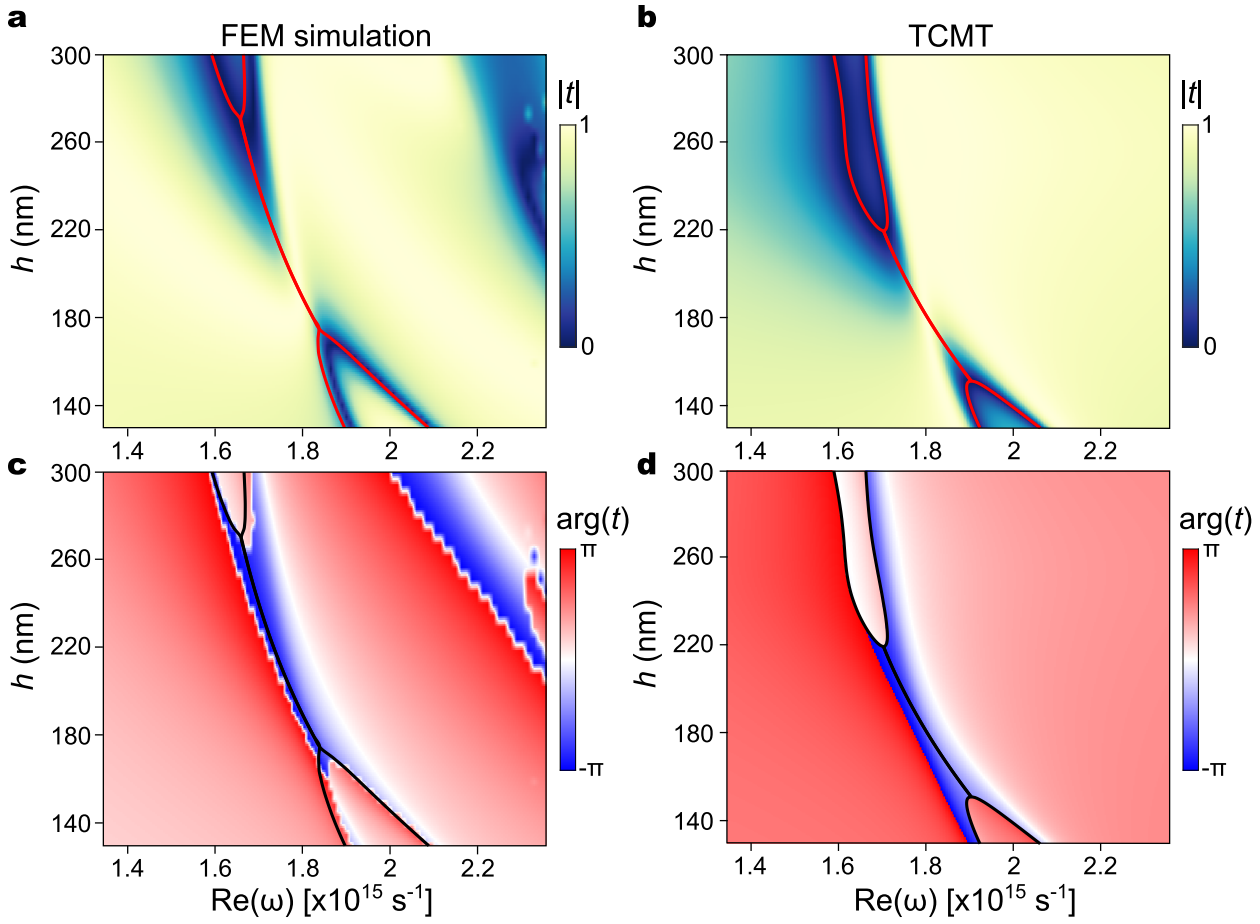

Supporting Fig. 2. Comparison of the **a** & **b**, amplitude and **c** & **d**, phase of the transmission coefficient as a function of real frequency and variable cylinder height h computed via an FEM calculation and TCMT [panels **b** & **d**, Eq. (24)]. The solid lines indicate the real part of the frequencies of the zeros in each case. The zeros for TCMT were calculated from Eq. (30).

Thus, replacing Eq. (22) in Eq. (14) and using Eq. (11), the scattering matrix is expressed as

$$S = \begin{pmatrix} r & t \\ t & r \end{pmatrix} = \begin{pmatrix} r_0 - \frac{(r_0+t_0')\gamma_1}{(-i\omega+i\omega_1+\gamma_1)} - \frac{(r_0-t_0')\gamma_2}{(-i\omega+i\omega_2+\gamma_2)} & t_0' - \frac{(r_0+t_0')\gamma_1}{(-i\omega+i\omega_1+\gamma_1)} + \frac{(r_0-t_0')\gamma_2}{(-i\omega+i\omega_2+\gamma_2)} \\ t_0' - \frac{(r_0+t_0')\gamma_1}{(-i\omega+i\omega_1+\gamma_1)} + \frac{(r_0-t_0')\gamma_2}{(-i\omega+i\omega_2+\gamma_2)} & r_0 - \frac{(r_0+t_0')\gamma_1}{(-i\omega+i\omega_1-\gamma_1)} - \frac{(r_0-t_0')\gamma_2}{(-i\omega+i\omega_2+\gamma_2)} \end{pmatrix}. \quad (23)$$

Note that the above scattering matrix corresponds to the case in which the first mode is even and the second is odd [cf. Eq. (22)]. The transmission and reflection coefficients are therefore given by

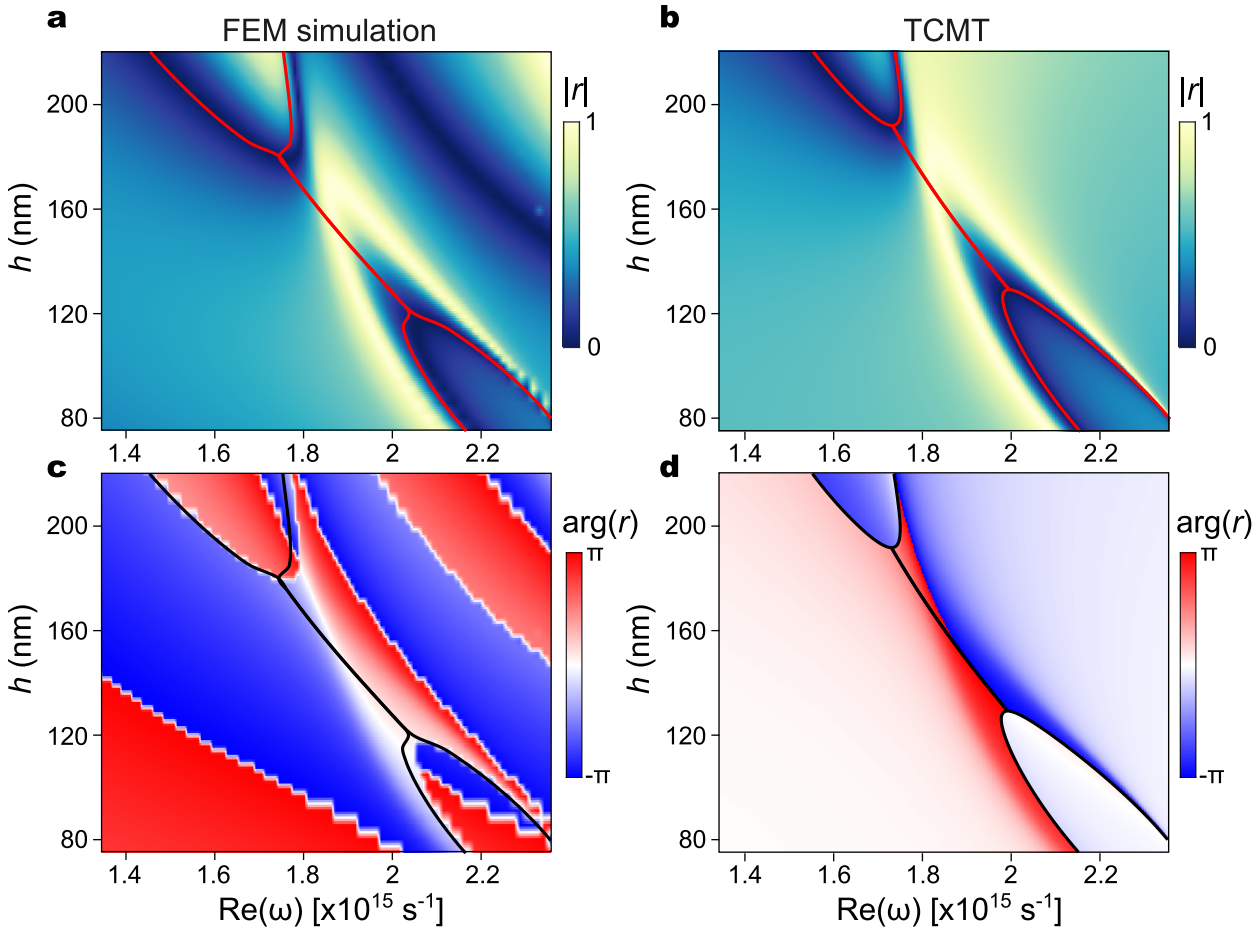

Supporting Fig. 3. Comparison of the **a** & **b**, amplitude and **c** & **d**, phase of the reflection coefficient as a function of real frequency and variable cylinder height h computed via an FEM calculation and TCMT [panels **b** & **d**, Eq. (25)]. The solid lines indicate the real part of the frequencies of the zeros in each case. The zeros for TCMT were calculated from Eq. (35).

$$t(\omega) = t_0' - \frac{(r_0 + t_0')\gamma_1}{(-i\omega + i\omega_1 + \gamma_1)} + \frac{(r_0 - t_0')\gamma_2}{(-i\omega + i\omega_2 + \gamma_2)}, \tag{24}$$

$$r(\omega) = r_0 - \frac{(r_0 + t_0')\gamma_1}{(-i\omega + i\omega_1 + \gamma_1)} - \frac{(r_0 - t_0')\gamma_2}{(-i\omega + i\omega_2 + \gamma_2)}. \tag{25}$$

B Calculation of the zeros from the scattering matrix

The zeros of the transmission coefficient above ($\tilde{\omega}^t_{\text{zero}}$) are given by the roots of the quadratic equation

$$a_t \left(\tilde{\omega}^t_{\rm zero}\right)^2 + b_t \tilde{\omega}^t_{\rm zero} + c_t = 0, \tag{26}$$

in which

$$a_t = -t'_0, \tag{27}$$

$$b_t = t'_0(\omega_1 + \omega_2) - ir_0(\gamma_2 - \gamma_1), \tag{28}$$

$$c_t = -t'_0(\omega_1\omega_2 + \gamma_1\gamma_2) - ir_0(\gamma_1\omega_2 - \gamma_2\omega_1). \tag{29}$$

Thus, the two zeros of the transmission coefficient are

$$\tilde{\omega}^t_{\rm zero,\pm} = \frac{-b_t \pm \sqrt{b_t^2 - 4a_t c_t}}{2a_t}. \tag{30}$$

From the above solution, we find that the two zeros are degenerate when the discriminant $\Delta = b_t^2 - 4a_t c_t = 0$, *i.e.*, when the following system of equations is satisfied

$$\begin{cases} (t'_0)^2(\omega_1 + \omega_2)^2 - \Big[r_0(\gamma_2 - \gamma_1)\Big]^2 - 4(t'_0)^2(\omega_1\omega_2 + \gamma_1\gamma_2) = 0, \\ (\omega_1 + \omega_2)(\gamma_2 - \gamma_1) + 2(\gamma_1\omega_2 - \gamma_2\omega_1) = 0. \end{cases} \tag{31}$$

One solution to the above equations is

$$\omega_2 = \omega_1, \tag{32}$$

$$\gamma_2 = \gamma_1\left[f_t(r_0, t'_0) \pm \sqrt{[f_t(r_0, t'_0)]^2 - 1}\right], \tag{33}$$

where $f_t(r_0, t'_0) = 1 - 2(t'_0/r_0)^2$.

The real degenerate transmission zeros are expressed as

$$\tilde{\omega}^t_{\rm zero,\ deg} = \frac{\omega_1 + \omega_2}{2} - \frac{ir_0}{2t'_0}(\gamma_2 - \gamma_1). \tag{34}$$

with $\omega_{1,2}$ and $\gamma_{1,2}$ satisfying Eq. (31).

The zeros of the reflection coefficient ($\tilde{\omega}^r_{\rm zero}$) of Eq. (25) are

$$\tilde{\omega}^r_{\rm zero,\pm} = \frac{-b_r \pm \sqrt{b_r^2 - 4a_r c_r}}{2a_r}. \tag{35}$$

in which

$$a_r = -r_0, \tag{36}$$

$$b_r = r_0(\omega_1 + \omega_2) - it_0'(\gamma_2 - \gamma_1), \tag{37}$$

$$c_r = -r_0(\omega_1\omega_2 + \gamma_1\gamma_2) - it_0'(\gamma_1\omega_2 - \gamma_2\omega_1). \tag{38}$$

The conditions ruling the pole frequencies at the reflection zero degeneracy are obtained by interchanging r_0 and t_0' in Eq. (31). Degenerate reflection zeros can occur for

$$\omega_2 = \omega_1, \tag{39}$$

$$\gamma_2 = \gamma_1\left[f_r(r_0, t_0') \pm \sqrt{[f_r(r_0, t_0')]^2 - 1}\right], \tag{40}$$

where $f_r(r_0, t_0') = 1 - 2(r_0/t_0')^2$ and the real degenerate reflection zeros are expressed as

$$\tilde{\omega}^r_{\text{zero, deg}} = \frac{\omega_1 + \omega_2}{2} - \frac{it_0'}{2r_0}(\gamma_2 - \gamma_1), \tag{41}$$

with $\omega_{1,2}$ and $\gamma_{1,2}$ satisfying Eqs. (39) and (40).

The transmission and reflection coefficients are calculated from Eqs. (24) and (25) for the considered metasurface geometry using the complex pole frequencies computed by an FEM electromagnetic simulation (see Methods in the main text). The real frequency response as a function of cylinder height for the transmission and reflection coefficients computed by an FEM simulation and from Eqs. (24) and (25) are shown in Supporting Fig. 2 and 3. As shown from the figures, the temporal coupled-mode theory calculations [Eqs. (24) and (25)] are in fair agreement with the FEM simulations. However, some of the behavior is absent from the TCMT calculation (see Supporting Fig. 2 and 3), which is associated with additional resonances that are unaccounted for in the current calculation. We note here that the temporal coupled-mode theory only captures spectral behavior around the frequencies of the poles that are used in the calculation. As such, it is expected that a higher degree of accuracy can be obtained by increasing the number of poles included in the calculation. The full evolution of the amplitudes of the transmission and reflection coefficients as a function of increasing cylindrical height h calculated by TCMT for complex and real frequencies can be found in visualizations 1 and 2 accompanying this supplemental document.

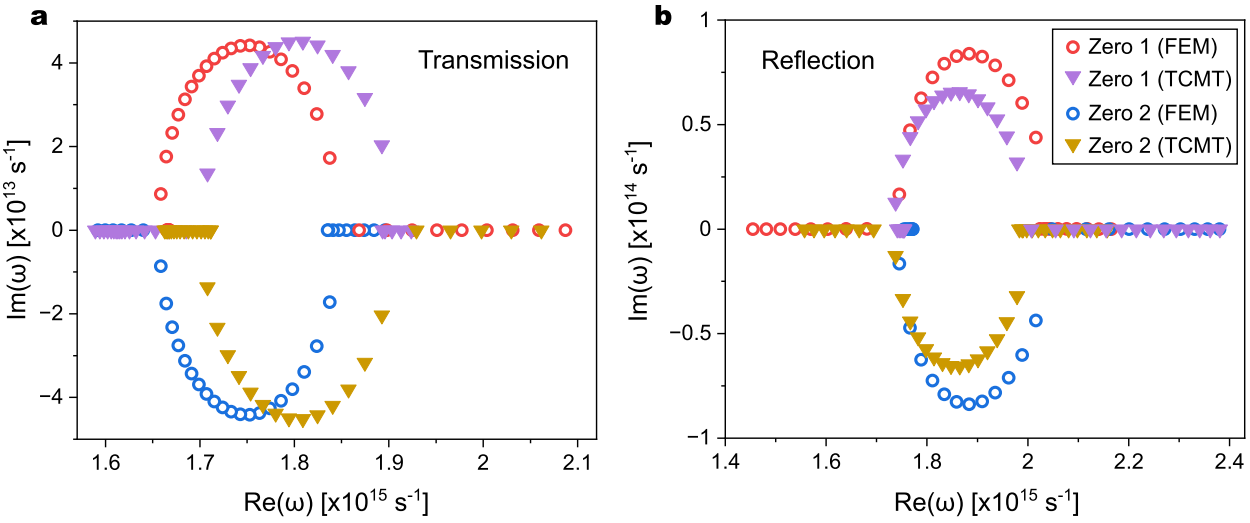

Supporting Fig. 4. Comparison of the complex frequencies of **a**, transmission and **b**, reflection zeros computed via an FEM simulation (see Methods) and TCMT (section III) as a function of increasing cylinder height h. For panel **a**, $h \in [130\,\text{nm}, 300\,\text{nm}]$ and for panel **b**, $h \in [75\,\text{nm}, 220\,\text{nm}]$.

The transmission and reflection zeros are calculated using Eqs. (30) and (35) and are compared to those obtained via finite-element method (FEM) calculations, showing fair agreement (see Supporting Fig. 4). A slight shift in the real frequency of the zeros calculated using TCMT is observed compared to that of the FEM calculation. The shift corresponds to a difference in wavelength $\Delta\lambda \simeq 30$ nm and $\Delta\lambda \simeq 10$ nm for transmission and reflection, respectively.

C The role of modal symmetry

For the case in which the two modes have the same symmetry, we confirm below that degenerate zeros can only occur in the presence of material loss and gain, indicating that the Kerker behavior is indeed associated with the interaction of modes with opposite symmetry. In the symmetric case, degenerate zeros arise when the loss and gain channels are in balance, which is a behavior that is again associated with $\mathcal{PT}$-symmetry[6].

The transmission coefficient for the case of two modes having the same symmetry is[5]

$$t' = t'_0 - \frac{(r_0 + t'_0)\left[(-i\omega + i\omega_2)\gamma_1 + (-i\omega + i\omega_1)\gamma_2\right]}{(-i\omega + i\omega_1 + \gamma_1)(-i\omega + i\omega_2 + \gamma_2) - \gamma_1\gamma_2} \tag{42}$$

The zeros of this transmission coefficient are

$$\tilde{\omega}^{t'}_{\text{zero}} = \frac{-b'_t \pm \sqrt{(b'_t)^2 - 4a'_t c'_t}}{2a'_t}. \tag{43}$$

in which

$$a'_t = -t'_0, \tag{44}$$

$$b'_t = t'_0(\omega_1 + \omega_2) + ir_0(\gamma_1 + \gamma_2), \tag{45}$$

$$c'_t = -t'_0\omega_1\omega_2 - ir_0(\gamma_1\omega_2 + \gamma_2\omega_1). \tag{46}$$

These zeros are degenerate if the following system of equations is satisfied

$$\begin{cases} (t'_0)^2(\omega_1 + \omega_2)^2 - \Big[r_0(\gamma_1 + \gamma_2)\Big]^2 - 4(t'_0)^2\omega_1\omega_2 = 0, \\ (\omega_1 + \omega_2)(\gamma_1 + \gamma_2) - 2(\gamma_1\omega_2 + \gamma_2\omega_1) = 0, \end{cases} \tag{47}$$

which yields the conditions

$$\omega_2 = \omega_1, \tag{48}$$

$$\gamma_2 = -\gamma_1. \tag{49}$$

Therefore, for two modes of the same symmetry, degenerate zeros only occur in the presence of loss and gain, particularly when the loss and gain channels are in balance, as indicated by Eq. (49). This is also the case for reflection.

IV The constrained Hamiltonian eigenvalue problem

In this section, we formulate an eigenvalue problem whose eigenvalues are the frequencies Ω that satisfy some constraint (*e.g.*, transmission or reflection zeros). The eigenvectors will be the modal mixtures yielding the desired scattering behavior. The constraint corresponds to a specific "target" scattering matrix: $s_- = Ss_+$. Using this scattering matrix to eliminate s_+ from the dynamical equations (8) and (9), we can re-write Eq. (8) in a form that is equivalent to the time-dependent Schrödinger equation, *i.e.*,[7]

$$i\frac{\mathrm{d}\Psi}{\mathrm{d}t} = H\Psi, \tag{50}$$

in which the Hamiltonian H satisfies the following eigenvalue problem [cf. Eq. (13)]

$$H(\Omega)\Psi = \Omega\Psi, \tag{51}$$

$$H(\Omega) = i\big\{ -i\Omega_0 - \Gamma + \kappa^{\mathrm{T}}[S(\Omega) - S_{\mathrm{d}}]^{-1}\kappa\big\}. \tag{52}$$

It is clear from the above equations that in the limit $\mathrm{Det}(S) \to \infty$ we obtain the usual Hamiltonian eigenvalue problem, *i.e.*, $-i\Omega\Psi = (-i\Omega_0 - \Gamma)\Psi$, where Ω gives the system's complex pole frequencies. The Hamiltonian of Eq. (52) is expressed as follows

$$H(\Omega) = H_0 + H'(\Omega), \tag{53}$$

where $H_0 = \Omega_0 - i\Gamma = \Omega_0 - i\kappa^{\dagger}\kappa/2$ is the interaction-free Hamiltonian giving the temporal evolution of the modes and $H'(\Omega) = i\big\{\kappa^{\mathrm{T}}[S(\Omega) - S_{\mathrm{d}}]^{-1}\kappa\big\}$ is the interaction Hamiltonian, which describes the scattering behavior.

For a two-mode, two-port photonic resonator, we write $S = \begin{pmatrix} S_{11} & S_{12} \\ S_{21} & S_{22} \end{pmatrix}$ and define $\Delta S = S - S_d = \begin{pmatrix} \Delta S_{11} & \Delta S_{12} \\ \Delta S_{21} & \Delta S_{22} \end{pmatrix} = \begin{pmatrix} S_{11} - r_0 & S_{12} - t_0' \\ S_{21} - t_0' & S_{22} - r_0 \end{pmatrix}$ so that

$$(S - S_d)^{-1} = \Delta S^{-1} = \begin{pmatrix} B_{11} & B_{12} \\ B_{21} & B_{22} \end{pmatrix} = \frac{1}{\Delta S_{11}\Delta S_{22} - \Delta S_{12}\Delta S_{21}} \begin{pmatrix} \Delta S_{22} & -\Delta S_{12} \\ -\Delta S_{21} & \Delta S_{11} \end{pmatrix}. \tag{54}$$

Using Eq. (22), we have

$$H' = i\kappa^{\mathrm{T}}(S - S_{\mathrm{d}})^{-1}\kappa = \begin{pmatrix} -iD_{11} & k_{12} \\ k_{21} & -iD_{22} \end{pmatrix}. \tag{55}$$

where

$$D_{11} = \gamma_1(r_0 + t_0')\big[(B_{11} + B_{21}) + (B_{12} + B_{22})\big], \tag{56}$$

$$k_{12} = i\sqrt{\gamma_1\gamma_2}\big[B_{11} + B_{21} - B_{12} - B_{22}\big], \tag{57}$$

$$k_{21} = i\sqrt{\gamma_1\gamma_2}\big[B_{11} - B_{21} + B_{12} - B_{22})\big], \tag{58}$$

$$D_{22} = \gamma_2(r_0 - t_0')\big[B_{11} - B_{21} - B_{12} + B_{22}\big]. \tag{59}$$

Note that the top signs in Eq. (22) were used above. Therefore, the Hamiltonian is given by

$$H = \begin{pmatrix} \omega_1 - i\tilde{\gamma}_1 & k_{12} \\ k_{21} & \omega_2 - i\tilde{\gamma}_2 \end{pmatrix}, \tag{60}$$

in which

$$\tilde{\gamma}_1 = \gamma_1 + D_{11}, \tag{61}$$

$$\tilde{\gamma}_2 = \gamma_2 + D_{22}. \tag{62}$$

Since in our TCMT derivation, we assume a nano-structure with mirror-symmetry, *i.e.*, $S_{11} = S_{22} = r(\omega)$ and $S_{12} = S_{21} = t(\omega)$, then from Eqs. (57) and (58) we have $k_{12} = k_{21} = 0$ so that the Hamiltonian is

$$H = \begin{pmatrix} \omega_1 - i\tilde{\gamma}_1 & 0 \\ 0 & \omega_2 - i\tilde{\gamma}_2 \end{pmatrix}, \tag{63}$$

with eigenvalues

$$\tilde{\omega}_1 = \omega_1 - i\tilde{\gamma}_1(\tilde{\omega}_1), \tag{64}$$

$$\tilde{\omega}_2 = \omega_2 - i\tilde{\gamma}_2(\tilde{\omega}_2), \tag{65}$$

where

$$\tilde{\gamma}_1(\tilde{\omega}_1) = \gamma_1 \left\{ 1 + 2\frac{(r_0 + t_0')\Big[r(\tilde{\omega}_1) - r_0 + t_0' - t(\tilde{\omega}_1)\Big]}{[r(\tilde{\omega}_1) - r_0]^2 + [t(\tilde{\omega}_1) - t_0']^2} \right\}, \tag{66}$$

$$\tilde{\gamma}_2(\tilde{\omega}_2) = \gamma_2 \left\{ 1 + 2\frac{(r_0 - t_0')\Big[r(\tilde{\omega}_2) - r_0 - t_0' + t(\tilde{\omega}_2)\Big]}{[r(\tilde{\omega}_2) - r_0]^2 + [t(\tilde{\omega}_2) - t_0']^2} \right\}. \tag{67}$$

The eigenvalues given in Eqs. (64) and (65) indicate that if scattering zeros are imposed in the Hamiltonian of Eq. (52), then the resulting eigenvalues correspond to those of the scattering zeros $\tilde{\omega}^{t,r}_{\text{zero},\pm}$. In Supporting Fig. 5, we show a comparison between the complex frequencies of transmission and reflection zeros [T- ($\tilde{\omega}^{t}_{\text{zero},\pm}$) and R-zeros ($\tilde{\omega}^{r}_{\text{zero},\pm}$)] obtained directly from the scattering matrix [Eqs. (23), (30), and (35)] and by injecting the zero frequencies

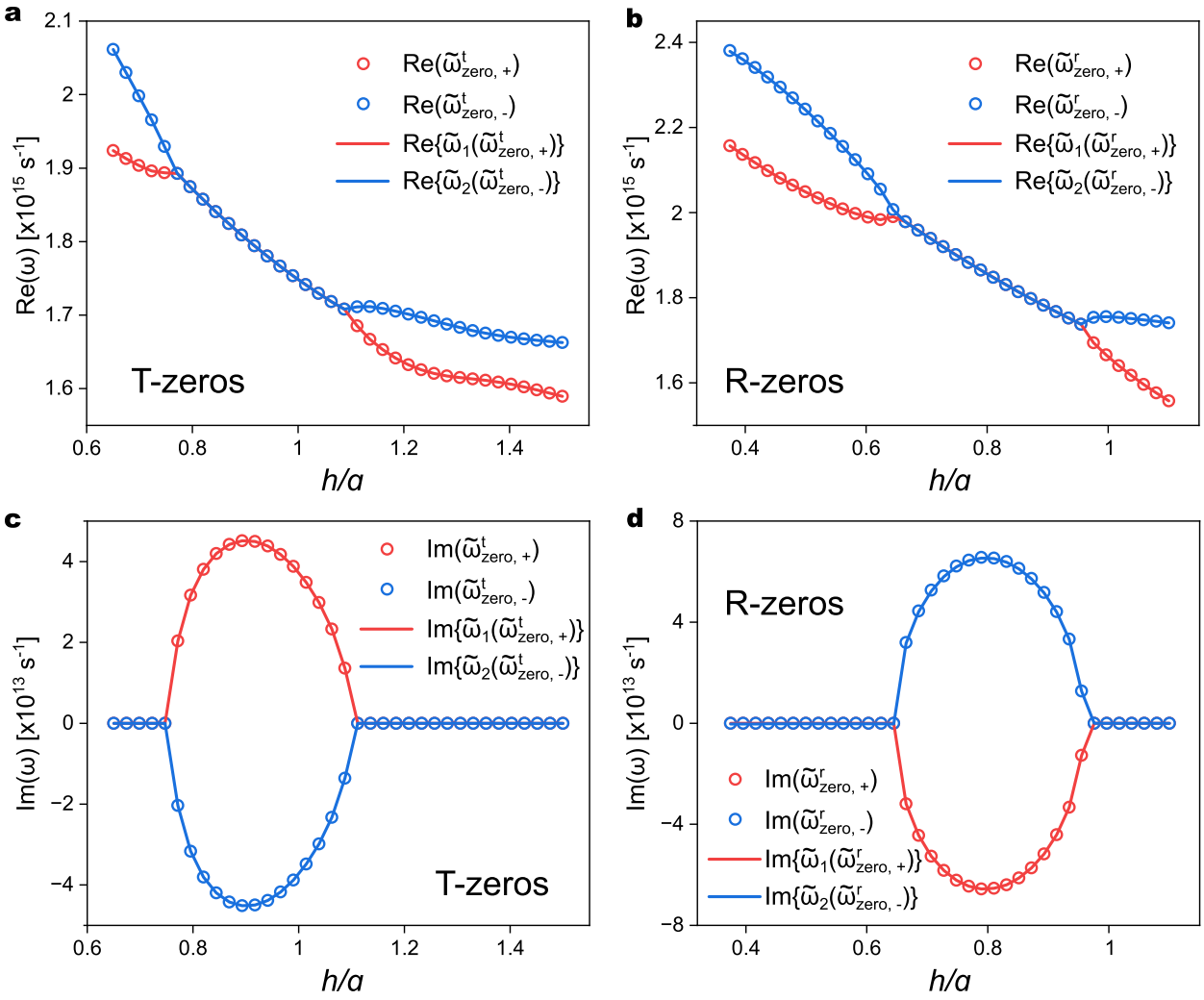

Supporting Fig. 5. **a & b**, Real and **c & d**, imaginary parts of T- and R-zeros as a function of the dimensionless geometric parameter h/a (h is the variable cylinder height and $a = 200$ nm is the cylinder radius), calculated directly from the scattering matrix [Eq. (23)], denoted by $\tilde{\omega}^{t,r}_{\text{zero},\pm}$ (hollow circles), and by injecting $\tilde{\omega}^{t,r}_{\text{zero},\pm}$ into the right-hand-sides of Eqs. (64) and (65) [solid lines], respectively.

[Eqs. (30) and (35)] into the right-hand-sides of Eqs. (64) and (65). The equivalence between the frequencies obtained from both methods validates the assumption that T- or R-zeros are recovered from the Hamiltonian eigenvalue problem [Eq. (51)] when constrained by scattering zeros.

The Hamiltonian is $\mathcal{PT}$-symmetric when it commutes with the parity-time operation, that is

$$\left[\mathcal{PT}, H\right] = (\mathcal{PT})H - H(\mathcal{PT}) = 0, \tag{68}$$

where $\mathcal{P}$ is the parity operator, which in the current case is the Pauli matrix $\sigma_x = \begin{pmatrix} 0 & 1 \\ 1 & 0 \end{pmatrix}$. The action of the time-reversal operator $\mathcal{T}$ is to take the complex conjugate of everything as well as interchanging the input and output channels. These operators satisfy the relations $\mathcal{P}^2 = 1$, $\mathcal{P} = \mathcal{P}^\dagger$, $\mathcal{T}^2 = 1$, $\mathcal{T} = \mathcal{T}^\dagger$, $\mathcal{P} = \mathcal{P}^{-1}$, $\mathcal{T} = \mathcal{T}^{-1}$, and $\left[\mathcal{P}, \mathcal{T}\right] = 0$. Thus, the $\mathcal{PT}$-symmetry condition of Eq. (68) can be rewritten as follows

$$H = (\mathcal{PT})H(\mathcal{PT}) \tag{69}$$

$$= \mathcal{P}H^*\mathcal{P} \tag{70}$$

From the above relation, we find that the Hamiltonian of Eq. (63) is $\mathcal{PT}$-symmetric if

$$\omega_1 - i\tilde{\gamma}_1(\tilde{\omega}_1) = \omega_2 + i\tilde{\gamma}_2^*(\tilde{\omega}_2) \quad \text{and} \quad \omega_2 - i\tilde{\gamma}_2(\tilde{\omega}_2) = \omega_1 + i\tilde{\gamma}_1^*(\tilde{\omega}_1). \tag{71}$$

When imposing transmissionless or reflectionless scattering, the eigenvalues of the constrained Hamiltonian are the zeros and thus follow the same complex plane behavior as the zeros. In the $\mathcal{PT}$-symmetry regime of the zeros, Eq. (71) is hence satisfied, and spontaneous $\mathcal{PT}$-symmetry-breaking occurs when Eq. (71) no longer holds.

Media

Two visualizations (visualizations 1 and 2) accompany this supporting information document. The visualizations show a TCMT calculation [Eqs. (24) and (25) of this supplementary information document] of the evolution of the nano-cylinder array's transmission (visualization 1) and reflection (visualization 2) coefficients as a function of cylinder height h. Each visualization has two panels: (left panel) complex plane behavior of the transmission or reflection coefficient; (right panel) real frequency response of the transmission or reflection coefficient.

References

1. Decker, M. *et al.* High-efficiency dielectric Huygens' surfaces. *Adv. Opt. Mater.* **3,** 813–820 (2015).

2. Markos, P. & Soukoulis, C. *Wave propagation: from electrons to photonic crystals and left-handed materials* (Princeton University Press, 2008).

3. Haus, H. Waves and fields in optoelectronics. *Prentice- Hall, Englewood Cliffs* (1984).

4. Fan, S., Suh, W. & Joannopoulos, J. Temporal coupled-mode theory for the Fano resonance in optical resonators. *J. Opt. Soc. Am. A* **20,** 569–572 (2003).

5. Suh, W., Wang, Z. & Fan, S. Temporal coupled-mode theory and the presence of non-orthogonal modes in lossless multimode cavities. *IEEE J. Quantum Electron.* **40,** 1511–1518 (2004).

6. Özdemir, Ş. K., Rotter, S., Nori, F. & Yang, L. Parity–time symmetry and exceptional points in photonics. *Nat. Mater.* **18,** 783–798 (2019).

7. Hsu, C., Zhen, B., Stone, A., Joannopoulos, J. & Soljačić, M. Bound states in the continuum. *Nat. Rev. Mater.* **1,** 1–13 (2016).